

Inversion of Two-Band Superconductivity at the Critical Electron Doping of $(\text{Mg}, \text{Al})\text{B}_2$

L. D. Cooley, A. J. Zambano, A. R. Moodenbaugh, R. F. Klie, Jin-Cheng Zheng, and Yimei Zhu

Brookhaven National Laboratory, Upton, New York 11973, USA

(Received 18 April 2005; published 27 December 2005)

Electron energy-loss spectroscopy (EELS) was combined with heat capacity measurements to probe changes of electronic structure and superconductivity in $\text{Mg}_{(1-x)}\text{Al}_x\text{B}_2$. A simultaneous decrease of EELS intensity from σ -band hole states and the magnitude of the σ gap was observed with increasing x , thus verifying that band filling results in the loss of strong superconductivity. These quantities extrapolated to zero at $x \approx 0.33$ as inferred from the unit cell volume. However, superconductivity was not quenched completely, but persisted with $T_c < 7$ K up to about $x \approx 0.55$. Only the π band had detectable density of states for $0.33 \lesssim x \lesssim 0.55$, implying an inversion of the two-band hierarchy of MgB_2 in that regime. Since π -band superconductivity is active in other materials such as intercalated graphite, implications for new materials with high T_c are discussed.

DOI: [10.1103/PhysRevLett.95.267002](https://doi.org/10.1103/PhysRevLett.95.267002)

PACS numbers: 74.70.Ad, 74.25.Jb, 74.62.Dh, 79.20.Uv

Although two-band superconductivity was first studied theoretically in 1959 [1], its detailed experimental study has not been possible until the discovery of superconductivity near 40 K in MgB_2 in 2001 [2]. The high critical temperature T_c results from two key ingredients: First, the boron σ band, which is deep beneath the Fermi energy E_F in graphite, sits just above the Fermi energy and provides a high density of p_{xy} hole states [3,4]. Second, the boron-boron E_{2g} bond oscillation is renormalized downward in energy (softened), into the range where the phonon coupling to the hole states is nearly perfect [5,6]. The 2D σ band carries along with it superconductivity in a 3D π band with p_z electron states, which has a smaller superconducting gap energy and weaker electron-phonon coupling [4].

Since the σ band appears to be so crucial to superconductivity, many experiments have attacked the central question of how superconductivity changes upon substituting Al or C for Mg or B, respectively, thereby providing extra electrons that fill its hole states. A common observation has been that such dopants destroy superconductivity [7–11]. For Al doping, $T_c(x)$ falls with increasing Al concentration x , sometimes increasing slope at $x \approx 0.3$ and reaching zero for $x = 0.5$ to 0.6 [8,12,13]. The loss of superconductivity at $x \approx 0.5$ correlates with changes seen in NMR data [14,15], optical reflectance [16], and infrared absorption [8]. Heat capacity measurements [17] show an approximately linear decrease of both gaps out to $x = 0.4$, suggesting that interband scattering does not affect these trends strongly. A rise of the Fermi level consistent with band filling has been inferred from x-ray absorption spectroscopy (XAS) [16], but quantitative data are not available.

Theoretical predictions are generally consistent with these observations, but also add unusual details. Electronic structure calculations within the virtual crystal approximation predict that the cylindrical Fermi surfaces attributed to the boron σ band collapse at the Γ point in reciprocal space when $x \approx 0.3$, separating the cylinders

into strings of ellipsoidal pockets [18]. Complete filling of the σ band holes was predicted to occur at $x = 0.56$. The topological change at $x = 0.3$ suggests that abrupt changes in the properties occur for somewhat lower Al content than observed in experiments. One such change predicted to occur within the two-band Eliashberg formalism [19,20] is a crossover in the hierarchy of superconducting gap energies for the two bands, with the π band becoming stronger than the σ band at high doping, opposite to the order for pure MgB_2 . In this region, the predicted T_c is also much lower than observed experimentally, perhaps due to uncertainty of the true amount of Al actually incorporated in the superconductor or the inhomogeneous distribution of Al.

In this Letter we present experimental data that validate these theoretical predictions better than in earlier work, including the inversion of the relative strength of superconductivity on the 2 bands when the Al content is high. We combine spectroscopy, which tracks the loss of hole states on the σ band, with heat capacity measurements, which provide information about the behavior of both gaps. We also analyze data in terms of the relative change of the unit-cell volume $\nu(x) = V(x)/V_0$, where $V_0 = V(0)$ is the unit-cell volume for pure MgB_2 , and $V(x)$ is the unit-cell volume obtained from x-ray diffraction data after reaction [21]. Since the crystal lattice changes systematically with added Al, this procedure gives a better volumetric representation of the Al content actually present, on average, in the superconducting phase. This procedure removes the scatter in data when plotted in terms of x , as summarized for instance in Ref. [22]. Thus, we obtain better insight to the physics beneath superconductivity in $\text{Mg}_{1-x}\text{Al}_x\text{B}_2$.

Two sets of samples were prepared using reactions at opposite limits of what is routinely used in the literature in terms of time and temperature: a short reaction “A,” 850 °C for 1 hr, which was stopped just short of full consumption of reactants (thus the superconducting phase is “as formed”); and a very hot, long reaction “B,”

1200 °C ramped down to 700 °C over >80 h like that in [23], which provided thorough annealing at the expense of a small loss of Mg or Al via diffusion along the interfaces where the reaction vessel was sealed. Full details of the structural characterization are described in [21].

It is important to note here that the crystal lattice parameters for sample set *B* generally obeyed a simple mixing rule between MgB_2 and AlB_2 end points (Vegard's law) and the composition measured after reaction by energy-dispersive x-ray spectroscopy in a scanning electron microscope. These samples thus appeared to be homogeneous in composition. Samples from set *A*, on the other hand, generally incorporated Al more slowly than Mg, and also displayed other signs of inhomogeneity. Yet, the effects of compositional inhomogeneity are mitigated by using Vegard's law to infer the composition from the x-ray diffraction data [21]. For instance, despite the evidence for inhomogeneity in one sample set, superconducting properties analyzed in terms of ν for both sets of samples fell onto a single curve, as for $T_c(\nu)$ shown in Fig. 1. This replotting eliminates the potential deviation that can occur when the actual Al content is not the nominal one. Uncertainty bars on this plot represent the 10% to 90% width of the T_c transition in a 1 mT background field, measured after cooling in zero field. The $T_c(\nu)$ curve exhibits a steep fall for $\nu > 0.96$, down to a critical temperature of about 7 K. For $\nu < 0.96$ the inductive transitions clearly showed bulk superconductivity, where in this region T_c extrapolates to 0 at $\nu \approx 0.93$ [21].

The large grain size produced by reaction *B* provided excellent samples to probe the electronic structure with electron energy-loss spectroscopy (EELS) [24,25]. We used a field-emission scanning transmission electron microscope (STEM) system used previously to probe the electronic structure of individual grains of pure MgB_2 [26]. EELS reduces the effects of surface contamination because the probe beam passes through the crystal volume.

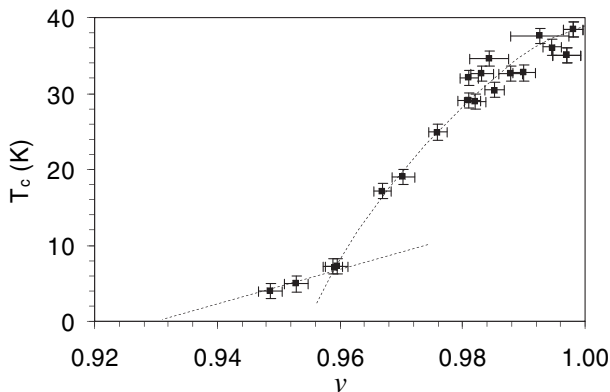


FIG. 1. Critical temperature as a function of the normalized volume of the unit cell taken from x-ray diffraction data [21]. The curves are guides to the eye. The axis along the top edge indicates Al concentration calculated for a simple rule of mixtures between MgB_2 and AlB_2 (Vegard's law).

Furthermore, special crystal orientations can be selected easily in the large thin area of a polycrystalline sample. Good correspondence between EELS and XAS was obtained in a study of the hole states in pure MgB_2 [27]. In the present experiment, we extend those analyses to Al-doped samples from set *B*.

The different natures of the electronic p_{xy} states and p_z states, which are associated with the σ band and the π band, respectively, lend a key advantage to the spectroscopy experiment. In pure MgB_2 , the p_{xy} density of states (DOS) has a steep edge as a function of energy, extending from several eV below E_F to about 0.9 eV above E_F [27]. The unoccupied p_{xy} states farther above E_F are few in number for about 5 eV, where a sharp rise in the p_{xy} DOS marks the main boron *K* edge. In contrast to these sharp features of the σ band, the p_z DOS is essentially constant with energy over that same range, providing a relatively constant background to the spectroscopy measurements. These differences are amplified further by using a large collection aperture and aligning the electron beam normal to the boron planes, which produces measured intensity that is dominated by the momentum transfer into p_{xy} states [26].

The essential features of the EELS data, shown in Fig. 2(a), are a prepeak at 186–189 eV energy loss followed by a strong series of peaks at 190 eV and above. Here, the spectra are aligned at 187 eV, which represents E_F . The prepeak is derived from core electrons being excited into the unoccupied p_{xy} states at the top of the σ band. As Al is added, a systematic loss of prepeak intensity occurs, indicating the rise of E_F into the flat portion of the σ band. This behavior is very similar to that measured by XAS [16], which included the intensity due to the p_z states. The main *K* edge also shifts downward, which will be described in a separate paper. A quantitative assessment of the p_{xy} DOS in this region as a function of doping was made by integrating the prepeak intensity and normalizing to the integrated intensity for $x = 0$. The inset of Fig. 2(a) shows the 2 different approaches used: First, a 2 eV wide Gaussian curve was fit to the peak intensity at approximately 187.5 eV, the width being due to the broadening of the STEM. Second, the tails of main edge peaks at ~ 192 and ~ 195 eV were fit by a 6 eV wide Gaussian [dashed curves in Fig. 2(a)] and subtracted, and the remaining intensity was integrated from 185 to 191 eV. As shown in the inset to Fig. 2(a), extrapolating either integrated intensity gives the Al content range where the σ band DOS becomes too small to contribute appreciable intensity, which evidently occurs for $x \geq 0.32$.

The STEM-EELS data are in good agreement with density-functional calculations based on the virtual crystal approximation, shown in Fig. 2(b). Here, the DOS calculations have been smoothed to simulate the broadening in the experiment. Figure 2(b) shows that there is no prepeak intensity for $x = 0.30$, at which point E_F intersects the σ band at the Γ point [Fig. 2(b) inset]. The remaining flat

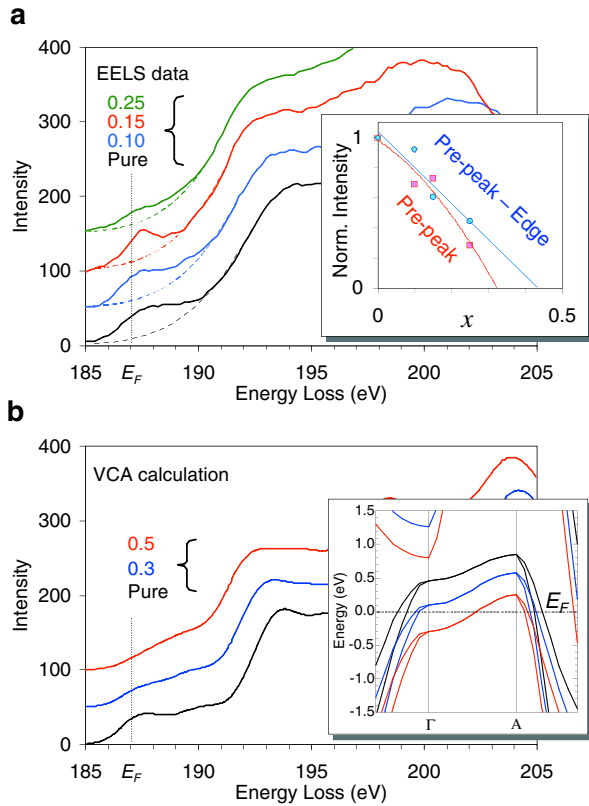


FIG. 2 (color online). STEM-EELS data are shown in plot (a). The dashed line indicates a Gaussian fit to peaks at higher energy, which was subtracted to estimate the prepeak intensity. The inset shows the normalized integrated intensity of the prepeak at 186–189 eV. Plot (b) shows simulated EELS spectra obtained by density-functional theory using the virtual crystal approximation. The inset shows the calculated band structure for the important σ band. In both plots (a) and (b), the Fermi energy is fixed and the curves are offset in intensity for clarity.

portion below 191 eV is due to the small amount of p_z states that are sampled by the simulated collection conditions, as indicated by the lack of any change in this region between $x = 0.30$ and $x = 0.50$. The overall calculations gave results very similar to those reported in [18], including the position of E_F relative to the bands as shown in the inset of Fig. 2(b).

Heat capacity measurements were coordinated with the EELS analyses to monitor the superconducting gaps for the σ and π bands, Δ_σ and Δ_π , and their DOS. Heat capacity data were collected using a commercial system and analyzed with a three-parameter fit (the so-called “alpha” model [28]) to extract the behavior of Δ_σ and Δ_π as a function of ν . Generally our data were very similar to those reported elsewhere [17,29].

The results of the alpha-model fitting [21] are shown in Fig. 3(a). These data show a strong decrease of Δ_σ with decreasing ν (i.e., with higher Al content). The π gap appears to hold constant for $\nu > 0.98$ and then decreases for smaller ν . However Δ_π remains well below Δ_σ until their values become equal at $\nu \approx 0.96$. This merging point

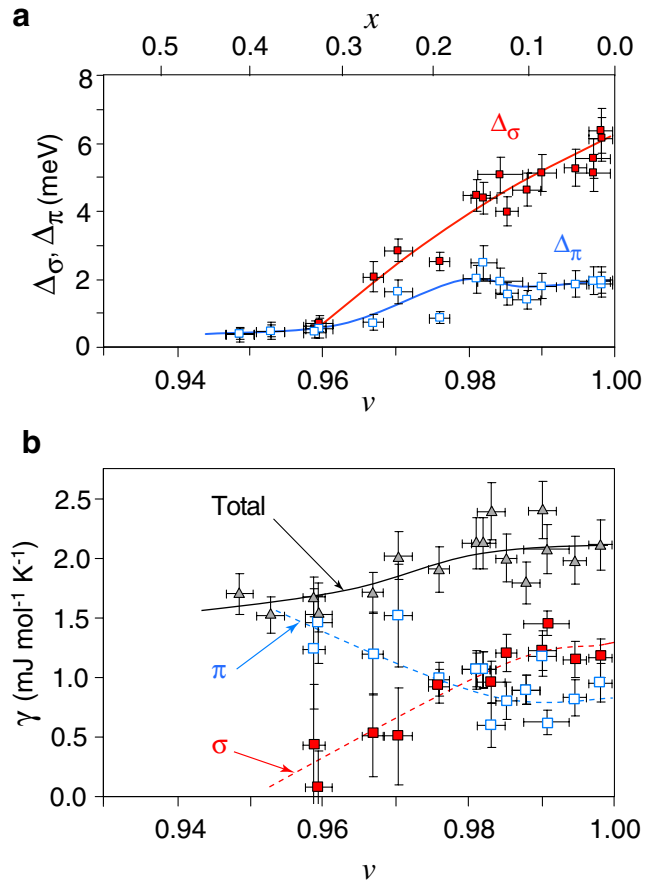


FIG. 3 (color online). The superconducting gaps for both sample sets extracted from heat capacity data are shown in plot (a). Curves are guides to the eye. The Sommerfeld coefficients extracted from the alpha-model fitting are shown in plot (b). Solid and dashed curves are guides to the eye.

corresponds to the unit-cell volume where the T_c data changes curvature rather sharply. The merging point of the gaps also corresponds to $x = 0.33$ according to Vegard’s law.

For still smaller ν , two gaps could not be distinguished, even though magnetization measurements demonstrate that bulk superconductivity survives, albeit only below 7 K. These data extrapolate to zero gap for $\nu \approx 0.93$ ($x \approx 0.55$ from Vegard’s law). The alpha model also provides information about the Sommerfeld coefficients for the bands, which are proportional to the individual DOS. Hence, the band responsible for this state can be inferred. In Fig. 3(b), it can be seen that a progressive loss of the σ band DOS occurs with decreasing ν (increasing x), extrapolating to zero for $\nu = 0.96$. By contrast, the π band DOS increases with ν . The σ and π DOS have approximately equal values at $\nu \approx 0.98$. These trends suggest that it is the π band that is the stronger band for $\nu < 0.96$, indicating a reversal of the two-band hierarchy in that regime.

We can summarize our results in terms of two important implications for understanding superconductivity in doped magnesium diborides. First, our data are generally more

consistent with the predictions of theory than the existing experimental studies on Al-doped MgB_2 . In particular, a much stronger rate of decrease of T_c and Δ_σ with composition (here derived from Vegard's law) has been found, indicating a stronger correlation between the loss of strong superconductivity on the σ band and the topological transition of the Fermi surface [30]. T_c falls from 39 to 7 K by the time E_F covers the σ band at the Γ point in reciprocal space (at $x \approx 0.33$), confirming the loss of Fermi-surface area as the primary factor for T_c in this region.

Second, for $0.33 \leq x \leq 0.55$ the system is essentially a π band superconductor with T_c values below 7 K. The complete loss of superconductivity at $x \approx 0.55$, when the σ band is filled completely, correlates with the loss of the soft zone-centered phonon modes in infrared absorption experiments [8,31]. However, coupling of the π band to these optical phonons is weak, making it unlikely that superconductivity could be sustained on the π band without a stronger σ band. We speculate that there must be coupling to other phonon branches that sustains the π band state. The situation may be similar to the π band coupling in intercalated graphite compounds such as CaC_6 [32].

In this sense, superconductivity in MgB_2 can be thought of as being derived from stable AlB_2 , where the π bonding keeps the position of the π band relatively fixed while the flat portion of the σ band is moved up through E_F by the addition of Mg. This implies that MgB_2 is not unique, but is an extraordinary member of the intercalated graphite family of superconductors. Since it is the π band that provides the bonding that anchors the layered structure, other superconductors with comparable T_c might therefore be possible by engineering the position of the σ band through doping. Alternatively, it might be possible to modify other diborides with stable π bonding, such as YB_2 , to produce superconductivity. Another interesting question is whether T_c continues to increase as the σ band moves upward away from E_F for Na or Li doping (if it is possible).

This work was supported by the U.S. Department of Energy, Office of Basic Energy Sciences under Grant No. DE-AC02-98CH10886. L. D. C and A. J. Z acknowledge additional support from BNL-LDRD programs. We would like to thank P. Canfield, A. Gurevich, J. Kortus, D. Larbalestier, W. Pickett, M. Suenaga, and D. Welch for stimulating discussions.

[1] H. Suhl, B. T. Matthias, and L. R. Walker, Phys. Rev. Lett. **3**, 552 (1959).

- [2] J. Nagamatsu, N. Nakagawa, T. Muranaka, Y. Zenitani, and J. Akimitsu, Nature (London) **410**, 63 (2001).
- [3] I. I. Mazin and V. P. Antropov, Physica C (Amsterdam) **385**, 49 (2003), and references therein.
- [4] H. J. Choi, D. Roundy, H. Sun, M. L. Cohen, and S. G. Loule, Nature (London) **418**, 758 (2002).
- [5] J. An and W. E. Pickett, Phys. Rev. Lett. **86**, 4366 (2001).
- [6] T. Yildirim *et al.*, Phys. Rev. Lett. **87**, 037001 (2001).
- [7] J. S. Slusky *et al.*, Nature (London) **410**, 343 (2001).
- [8] P. Postorino *et al.*, Phys. Rev. B **65**, 020507 (2002).
- [9] S. M. Kazakov *et al.*, Phys. Rev. B **71**, 024533 (2005).
- [10] R. A. Ribeiro, S. L. Bud'ko, C. Petrovic, and P. C. Canfield, Physica C (Amsterdam) **385**, 16 (2003); W. Mickelson, J. Cumings, W. Q. Han, and A. Zettl, Phys. Rev. B **65**, 052505 (2002).
- [11] R. H. T. Wilke *et al.*, Phys. Rev. Lett. **92**, 217003 (2004).
- [12] H. Luo, C. M. Li, H. M. Luo, and S. Y. Ding, J. Appl. Phys. **91**, 7122 (2002).
- [13] J. Q. Li *et al.*, Phys. Rev. B **65**, 132505 (2002).
- [14] S. Serventi *et al.*, Phys. Rev. B **67**, 134518 (2003).
- [15] G. Papavassiliou *et al.*, Phys. Rev. B **66**, 140514 (2002).
- [16] H. D. Yang *et al.*, Phys. Rev. B **68**, 092505 (2003).
- [17] M. Putti, M. Affronte, P. Manfrinetti, and A. Palenzona, Phys. Rev. B **68**, 094514 (2003).
- [18] O. de la Pena, A. Aguayo, and R. de Coss, Phys. Rev. B **66**, 012511 (2002).
- [19] A. Bussmann-Holder and A. Bianconi, Phys. Rev. B **67**, 132509 (2003).
- [20] G. A. Ummarino, R. S. Gonnelli, S. Massidda, and A. Bianconi, Physica C (Amsterdam) **407**, 121 (2004).
- [21] A. J. Zambano, A. R. Moodenbaugh, and L. D. Cooley, Supercond. Sci. Technol. **18**, 1411 (2005).
- [22] J. Kortus, O. V. Dolgov, R. K. Kremer, and A. A. Golubov, Phys. Rev. Lett. **94**, 027002 (2005).
- [23] M. H. Badr and K.-W. Ng, Supercond. Sci. Technol. **16**, 668 (2003).
- [24] R. F. Egerton, *Electron Energy Loss Spectroscopy in the Electron Microscope* (Plenum, New York, 1986).
- [25] N. D. Browning, M. F. Chisholm, and S. J. Pennycook, Nature (London) **366**, 143 (1993).
- [26] R. F. Klie *et al.*, Phys. Rev. B **67**, 144508 (2003).
- [27] Y. Zhu *et al.*, Phys. Rev. Lett. **88**, 247002 (2002).
- [28] Y. Wang, T. Plackowski, and A. Junod, Physica C (Amsterdam) **355**, 179 (2001).
- [29] F. Bouquet, R. A. Fisher, N. E. Phillips, D. G. Hinks, and J. D. Jorgensen, Phys. Rev. Lett. **87**, 047001 (2001).
- [30] A. Bianconi *et al.*, Phys. Rev. B **65**, 174515 (2002).
- [31] D. Di Castro *et al.*, Europhys. Lett. **58**, 278 (2002).
- [32] M. Calandra and F. Mauri, Phys. Rev. Lett. **95**, 237002 (2005).